

Spring Loaded Double Pantograph: A Robotic Mechanism for Safe Balance Training

Abstract—A Spring Loaded Double Pantograph (SLDP) mechanism is presented for safe balance training in elderly individuals practicing Tai Chi exercises. As people age, maintaining balance becomes increasingly critical, yet fear of falling often prevents effective exercise, creating a counterproductive cycle that increases fall risk. This natural hesitation to push physical limits during solo practice highlights the need for reliable safety systems. This paper presents a mechanism that provides variable assistance through spring-loaded actuation, so that support and freedom of movement can be balanced in a way that is both effective and unobtrusive. Here, it will be shown that, although support and unrestricted movement are traditionally considered contradictory goals, the two can be achieved simultaneously through mechanical design and the level of assistance can be automatically regulated. In this system, the support mechanism can a) detect falls rapidly, b) provide up to 98.0% body weight support when needed, and c) remain imperceptible during normal exercise. First, the mechanical design principles and kinematic analysis of the double-pantograph structure are presented. Methods for experimental validation with 13 human subjects will be addressed, demonstrating the system’s effectiveness through quantitative metrics of support forces, workspace utilization, and energy efficiency during simulated falls in Tai Chi movements.

I. INTRODUCTION

As we age, maintaining balance becomes increasingly critical for independence and quality of life [4]. Regular balance exercises, particularly Tai Chi, significantly reduce fall risk and improve mobility in older adults [1]–[3]. However, many individuals, particularly those exercising alone, hesitate to push themselves to their full potential due to fear of falling. This creates a counterproductive cycle - the fear of falling prevents effective challenge-based training, which in turn increases fall risk.

Imagine practicing challenging balance exercises with complete peace of mind - even as we age - knowing that an invisible safety net will catch you if you stumble, yet never interfere with your natural movements. For older adults, this means pushing physical limits without the constant fear of falling. This seamless integration of human motion and robotic support represents a fundamental challenge in rehabilitation robotics: how do we create support systems that remain imperceptible during normal movement, yet provide instant protection when needed? Such a system could transform how aging individuals approach balance training, enabling more effective exercise programs and ultimately reducing fall risk in our growing elderly population.

Current robotic support systems struggle with three key challenges: maintaining natural movement patterns, providing variable assistance based on user needs, and ensuring rapid response to potential falls. To address these challenges,



Fig. 1: A Tai Chi expert demonstrating traditional movements [38]. These movements illustrate the range of motion and support requirements that informed our system design and guided the development of the SLDP mechanism.

we propose a Spring Loaded Double Pantograph (SLDP) mechanism that provides variable assistance to the user’s movements and balance needs in real-time. Unlike traditional systems, the SLDP allows for unrestricted movement in three dimensions while maintaining supportive capabilities.

The key contributions of this paper are:

- 1) Mechanism Design: A Spring Loaded Double Pantograph (SLDP) mechanism, combining double-pantograph linkage with spring-loaded actuation to provide adaptive support while preserving natural movement patterns.
- 2) Physical Prototype: A physical system capable of supporting users up to 100 kg within a workspace of 0.4 to 1.1m radius and 128.9° arc.
- 3) Experimental Validation: Evaluation of the system with 13 human subjects performing Tai Chi exercises through simulated falls. Our experiments quantitatively validate that the system supported up to 98.0% of user weight during falls while maintaining unrestricted movement during normal exercise.

II. RELATED WORK

A. Basic Mechanisms

The pantograph mechanism has a rich history in handling heavy loads while maintaining precision. Early applications in industrial cranes by Walter et al. [6] demonstrated its effectiveness in load manipulation, while Gostling’s work [7] established fundamental principles for gravity compensation in pantograph-based systems. These early developments highlighted the mechanism’s inherent mechanical advantage and workspace flexibility.

Pioneering work by Hirose [11] in robotic locomotion further advanced the concept through three-dimensional Cartesian-coordinate pantograph mechanisms, demonstrating

their capabilities for precise motion control and energy efficiency. This work established fundamental principles of gravitationally decoupled actuation using pantograph structures, providing crucial insights into mechanism design for complex spatial movements. Building on this, researchers explored pantograph applications in various domains - from large-scale construction manipulators [8] to precise surgical instruments [9]. The mechanism's ability to maintain force relationships while scaling movements made it particularly suitable for tasks requiring both strength and precision.

Hirose's work focused primarily on single pantograph mechanisms for robotic manipulation and quadruped locomotion, without addressing human support applications. The mechanisms lacked the adaptive compliance needed for safe human interaction. Similarly, while industrial applications demonstrated the pantograph's load-bearing capabilities [6], they weren't designed for the dynamic and unpredictable nature of human movement support.

B. Human Support Systems

Existing robotic support systems can be categorized into:

- **Cable-Driven Support Systems:** FLOAT [28] and ZeroG [29] use overhead cables to provide body weight support. While they offer more freedom than exoskeletons, they are typically limited to a fixed workspace and struggle with support across varied motion patterns.
- **Lower-Limb Rehabilitation Robots:** Devices such as the Lokomat [30] and LOPES [31] are effective for gait training but are often confined to treadmill-based setups and neglect upper body movements.
- **Balance-Assisting Wearable Devices:** Lighter systems like the BalanceAid [32] and the Smart Belt [33] provide sensory augmentation or minimal physical support. However, they may offer insufficient assistance for users with significant balance impairments.
- **Soft Exosuits:** More recent developments like the Harvard Wyss Institute's soft exosuit [34] offer improved compliance compared to rigid exoskeletons. However, current designs are limited in their ability to support three-dimensional movements and provide variable levels of assistance across different body segments.
- **Robotic Walker Assistants:** Advanced walkers like the JAIST active robotic walker [35] provide mobile support but typically constrain the user's arm movements and are not suitable for exercises requiring full-body motion.

These limitations stem from fundamental design approaches that prioritize either support or freedom of movement, but struggle to effectively balance both. Our proposed SLDP mechanism addresses these limitations by providing adaptive support while maintaining natural movements.

III. SYSTEM OBJECTIVES

Through observational study of Tai Chi movements [38] [39] [40] and expert demonstrations (Fig. 1), we identified core principles:

- The practitioner moved freely in all directions, demonstrating unrestricted natural movements

- The practitioner maintained balance by shifting weight between stances with providing appropriate self-support
- When teaching patients, a human assistant observed the practitioner's demonstrations while staying ready to catch them if they lost balance during practice

From these principles, we determined three system objectives for supporting elderly or physically impaired users during exercise:

- 1) **Maintain Natural Movement:** Enable unrestricted motion in three-dimensional space without constraining the user's movement patterns
- 2) **Provide Adaptive Support:** Deliver variable assistance that matches the user's changing support needs during weight shifts and transitions
- 3) **Fall Protection:** Detect and respond rapidly to loss of balance while remaining unnoticeable during normal movement

IV. MECHANISM

The Spring Loaded Double Pantograph (SLDP) mechanism, illustrated in Fig. 2, introduces our approach to adaptive support for human movements in three-dimensional space. This design combines a double-pantograph linkage with spring-loaded actuation at point B to support the payload at point I. The 3D configuration enables the end effector to move freely in X, Y, and Z axes while maintaining key geometric constraints, with points B, J and F remaining collinear throughout the motion. This design creates a spherical workspace that supports multi-planar movements essential for dynamic balance exercises such as Tai Chi.

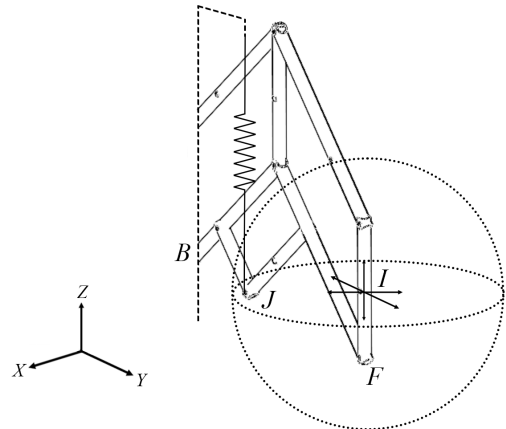
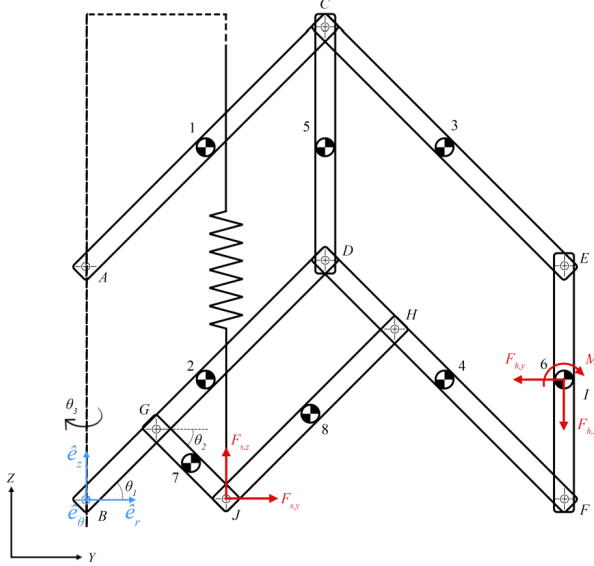


Fig. 2: SLDP mechanism in 3D

V. ANALYSIS

A. Kinematic Analysis

The kinematic diagram of the SLDP mechanism is illustrated in Figure 3. A key feature of the SLDP's design is the parallel arrangement of certain links - specifically, links 7, 4, and 3 are parallel to each other, as are links 2, 8, and 1. In this configuration, external forces acting at joints J and I



Nomenclature	
g	gravity vector
K	spring stiffness parameter
m	counterweight mass
M_h	joint reaction moment magnitude
N	Total number of mechanism Degrees of Freedom
ω	angular velocity
$F_{h,z}$	human force in \hat{e}_z direction
$F_{h,y}$	human force in \hat{e}_r direction
$F_{s,z}$	spring force in \hat{e}_z direction
$F_{s,y}$	spring force in \hat{e}_r direction
L_2	link 2 length
L_4	link 4 length
L_6	link 6 length
θ_1	angle from horizontal to link 2
θ_2	angle from horizontal to link 7
θ_3	angle from Y axis to plane of mechanism

Fig. 3: Definition of coordinate systems and kinematic parameters with accompanying nomenclature

are denoted in red, representing the interaction points with the user and the environment.

We introduce a rotating reference frame at point B. In this frame, unit vectors \hat{e}_r , \hat{e}_θ , and \hat{e}_z move with the mechanism, with \hat{e}_θ always remaining orthogonal to link 2 and rotating at a constant angular velocity $\dot{\theta}_3$.

We derive an expression for the position vector of Point I (the end effector) relative to Joint B. Using the geometry of the linkage, we obtain:

$$\bar{r}_I = L_2 \begin{pmatrix} \cos \theta_1 \\ \sin \theta_1 \end{pmatrix} + L_4 \begin{pmatrix} \cos \theta_2 \\ -\sin \theta_2 \end{pmatrix} + \frac{L_6}{2} \begin{pmatrix} 0 \\ 1 \end{pmatrix} \quad (1)$$

In this expression, L_2 and L_4 represent the lengths of their respective links, while θ_1 and θ_2 are the angles these links make with the horizontal. The term $\frac{L_6}{2}$ accounts for the half-length of link 6, which connects to the end effector.

To analyze the velocity of the end effector, we first consider the case where $\theta_3 = 0$, effectively analyzing the motion in the YZ plane. Differentiating Equation (1) with respect to time yields:

$$\vec{v}'_I = \begin{bmatrix} -L_2 \sin \theta_1 & -L_4 \sin \theta_2 \\ L_2 \cos \theta_1 & -L_4 \cos \theta_2 \end{bmatrix} \begin{pmatrix} \dot{\theta}_1 \\ \dot{\theta}_2 \end{pmatrix} \quad (2)$$

This equation expresses the end effector velocity, \vec{v}'_I , as a function of the angular velocities $\dot{\theta}_1$ and $\dot{\theta}_2$, with the matrix representing the Jacobian for this two-dimensional case.

To extend our analysis to three dimensions, we introduce rotation around the Z-axis. Setting $\dot{\theta}_3 = \omega \hat{e}_z$ (with $\dot{\omega} = 0$) and differentiating Equation (1) again, we obtain:

$$\vec{v}_I = \begin{bmatrix} -L_2 \sin \theta_1 & -L_4 \sin \theta_2 & 0 \\ 0 & 0 & -L_2 \cos \theta_1 \\ L_2 \cos \theta_1 & -L_4 \cos \theta_2 & 0 \end{bmatrix} \begin{pmatrix} \dot{\theta}_1 \\ \dot{\theta}_2 \\ \dot{\theta}_3 \end{pmatrix} \quad (3)$$

This three-dimensional velocity equation now includes components in the \hat{e}_r , \hat{e}_θ , and \hat{e}_z directions, describing the motion of the end effector in 3D space.

The workspace of the SLDP is defined by the ranges of the angles θ_1 and θ_2 . Both angles are constrained to the domain $[0, \pi]$. These constraints arise from the physical limitations of the mechanism:

$$0 \leq \theta_1, \theta_2 \leq \pi \quad (4)$$

It's important to note that these workspace calculations do not account for the physical constraint imposed by the spring. In practice, an additional constraint would be applied such that:

$$\theta_1 + \theta_2 < \pi \quad (5)$$

This constraint is necessary because the spring only engages when the end effector reaches the horizontal formed by the y-axis. At the point where $\theta_1 + \theta_2 = \pi$, the end effector would lie on the y-axis, defining the limit of the mechanism's range of motion.

B. Workspace Analysis

We analyzed the SLDP mechanism's workspace through both simulation and experimental validation. The simulated analysis, shown in Fig. 4, maps the workspace by varying joint angles θ_1 and θ_2 in the YZ-plane, and rotating through $\theta_3 [-\pi/2, \pi/2]$ to generate the full three-dimensional spherical workspace.

C. Static Analysis

The primary external forces acting on the system are the human interaction force ($F_{h,z}$) at point I and the spring force ($F_{s,z}$) at point J (see Fig. 3). Due to the double-pantograph

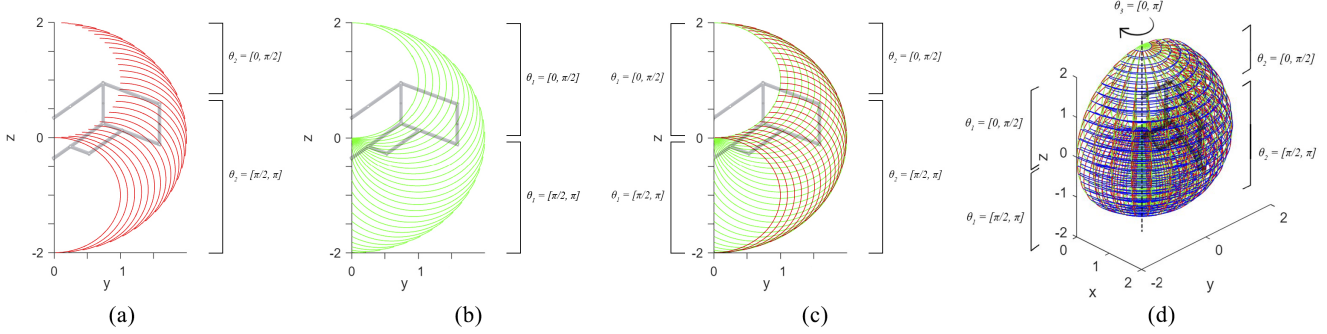


Fig. 4: Simulated workspace for the end effector. Subfigure (a) demonstrates the various sweeps of the end effector in the yz -plane as a function of θ_1 . A singular sweep represents the position of the end effector as a function of θ_1 in the domain $[0, \pi]$ while θ_2 remains at a set value within the range $[0, \pi]$. We form the whole workspace when we iterate through various discrete values of θ_2 in a linearly spaced set in the domain $[0, \pi]$. The labels on the z -axis denote the general area in which θ_2 corresponds to the given set of values. Subfigure (b) demonstrates the various sweeps of the end effector in the yz -plane as a function of θ_2 . The process is repeated with θ_1 remaining at a set value within the range $[0, \pi]$. While θ_2 continuously sweeps through the domain $[0, \pi]$. Subfigure (c) demonstrates the entire workspace of the end effector in the two-dimensional yz -plane as both a function of θ_1 and θ_2 . The labels on the y and z -axis denote the regions in which θ_1 and θ_2 are at a set, discrete values. Subfigure (d) demonstrates the full three-dimensional workspace of the end effector as a function of θ_1 , θ_2 , and θ_3 . A singular sweep in the xy -plane (shown in blue) represents the position of the end effector as a function of θ_3 in the domain $[\pi/2, -\pi/2]$ while θ_1 and θ_2 remain at set values.

geometry and parallel link arrangements, these forces are coupled through a mechanical advantage relationship:

$$F_{s,z} = \alpha F_{h,z} \quad (6)$$

where α is the mechanical advantage factor determined by the mechanism's configuration. This relationship ensures that the spring provides proportional support based on the user's needs, with the support force automatically adjusting as the configuration changes.

The static equilibrium of the system is maintained through a network of internal forces transmitted through the parallel linkages, with the spring force effectively counterbalancing external loads while maintaining system stability. At joint J where the spring force is applied:

$$F_{s,z} + T_7 \sin \theta_2 + T_8 \sin \theta_1 = 0 \quad (7)$$

The complete static analysis, including detailed force balance equations for all links and joints, is provided in our online appendix ¹.

VI. SYSTEM

Figure 6 shows the fabricated SLDP mechanism and its supporting hardware. A column-type load cell is placed on the wire supporting the device in order to measure the load applied. Three encoders are placed at joints B and J on the XZ-plane, as well as the XY-plane on at joint B to observe θ_1 , θ_2 , and θ_3 . The end effector at joint I attaches to the human subject via a swivel and harness so that the user can maintain full freedom of motion.

¹Static Analysis: <https://spring-loaded-double-pantograph-robot.github.io/static-analysis/>

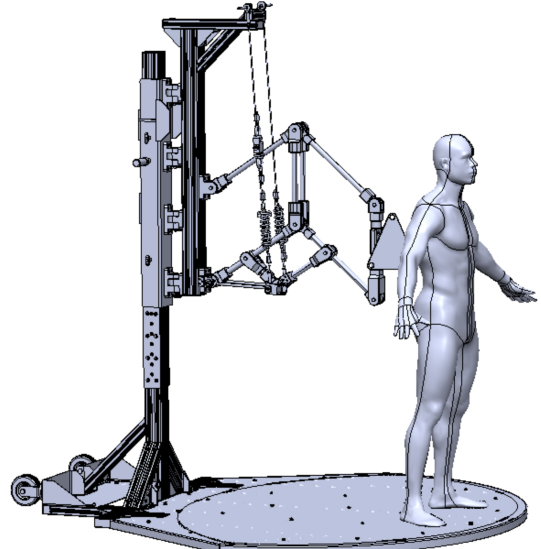


Fig. 5: Computer-aided design (CAD) model showing the SLDP system with support structure, mechanical linkages, and instrumentation placements ². The model illustrates key components including the double-pantograph mechanism, spring loading system, and sensor locations. A physical implementation of this design is shown in Figure 6.

The design process began with Computer-aided design (CAD) modeling, as shown in Figure 5, which enabled optimization of joint mechanisms, sensor placements, and safety features before physical construction. We utilized carbon fiber tubes for the primary linkages due to their exceptional strength-to-weight ratio. The main support links

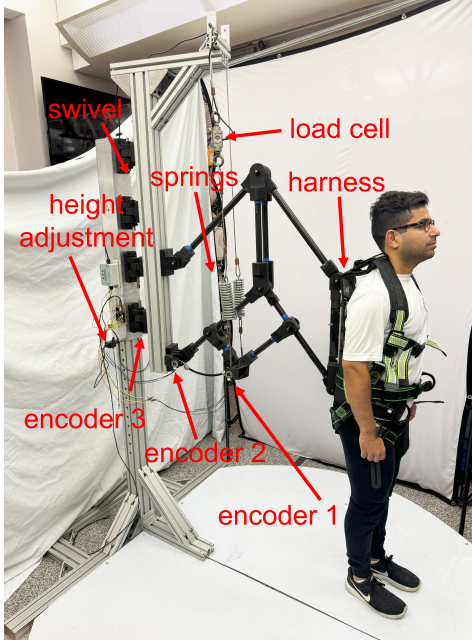


Fig. 6: Diagram of the physical system with a user. Mechanical elements and data collection devices are labeled in red.

(L_1, L_2, L_3, L_4) measure 441 mm in length with a 30 mm diameter. The end effector link (L_6), measuring 322 mm, was specially reinforced to handle direct user interactions.

Custom aluminum joint housings and precision ball bearings were integrated at all rotating joints to ensure smooth, low-friction operation. The links are connected through custom-made FDM 3D printed parts with a micro carbon fiber-filled nylon and solid infill to support large payloads.

Maximum Payload (kg)	100
Maximum Radius (m)	1.1
Minimum Radius (m)	0.4
Maximum Sweep Angle (°)	128.9
Spring Constant (kN/m)	73
Overall Mass (kg)	11.3

TABLE I: Mechanical System Parameters

We installed a high-precision column-type load cell with 700kg capacity and a digital amplifier with 0.1 N resolution to measure support forces, along with three rotary shaft encoders with 14-bit resolution and quadrature encoding strategically placed to monitor the critical angles θ_1 , θ_2 , and θ_3 .

Our prototype's key mechanical parameters are summarized in Table I. The system supports a maximum payload of 100 kg while maintaining a relatively light overall mass of 11.3 kg. The mechanism operates within a workspace defined by a maximum radius of 1.1 m and a vertical range from 0.2 m to 1.8 m above ground level. The spring system, tuned with an effective constant of 73 kN/m, provides responsive support with less than 100 ms reaction time while maintaining position accuracy within ± 2 mm at the end effector.

For human interface, we attached an ergonomic harness at joint I that combines safety with mobility. The harness

features adjustable straps and quick-release mechanisms, distributing support forces across the upper body while allowing natural arm and torso movements.

VII. EXPERIMENTATION

We conducted human subject testing to evaluate the effectiveness of the SLDP mechanism in providing support during Tai Chi exercises. The study protocol was approved by the Institutional Review Board (IRB Protocol #2212000845R001).

A. Experimental Setup

The SLDP mechanism was equipped with three encoders monitoring joint angles ($\theta_1, \theta_2, \theta_3$) and a load cell measuring vertical support force. Ground reaction forces were measured using force-sensitive insole resistors attached to the subjects' shoes. The data acquisition system sampled all sensors at 1 kHz, while a synchronized video recording system captured movement data for detailed analysis.

B. Subject Demographics

Thirteen subjects (8 male, 5 female) participated in the study, aged between 18-35 years with mean weight 64 ± 8 kg and height range 165-180 cm. The participants represented varying levels of Tai Chi experience, with two each at beginner, intermediate, and advanced levels. None had prior balance impairments.

C. Experimental Protocol

Each subject performed three 60-second trials comprising three components. First, subjects executed standard Tai Chi movements including Wave Hands Like Clouds, Grasp Bird's Tail, and Single Whip. Second, they performed intentional balance perturbations consisting of two to three staged falls per trial in various directions (forward, backward, lateral), with timing unknown to the system. Finally, subjects completed free-form movements within the workspace.

VIII. EVALUATION

A. Metrics

We define the following metrics in order to evaluate the performance:

- 1) **SLDP Support Fraction** is defined as:

$$R_{SLDP} := \frac{F_{s,z}}{\alpha W_h} \quad (8)$$

where W_h is the weight of the human, $F_{s,z}$ is the measured restoring spring force, and α is the mechanical advantage factor of the pantograph. This provides a dimensionless measure of the fraction of user weight supported by the device during a fall event.

- 2) **Foot Support Fraction** is defined as:

$$R_{Foot} := \frac{\int_{A_L} P_L dA + \int_{A_R} P_R dA}{W_h} \quad (9)$$

where:

²Design: <https://spring-loaded-double-pantograph-robot.github.io/design/>

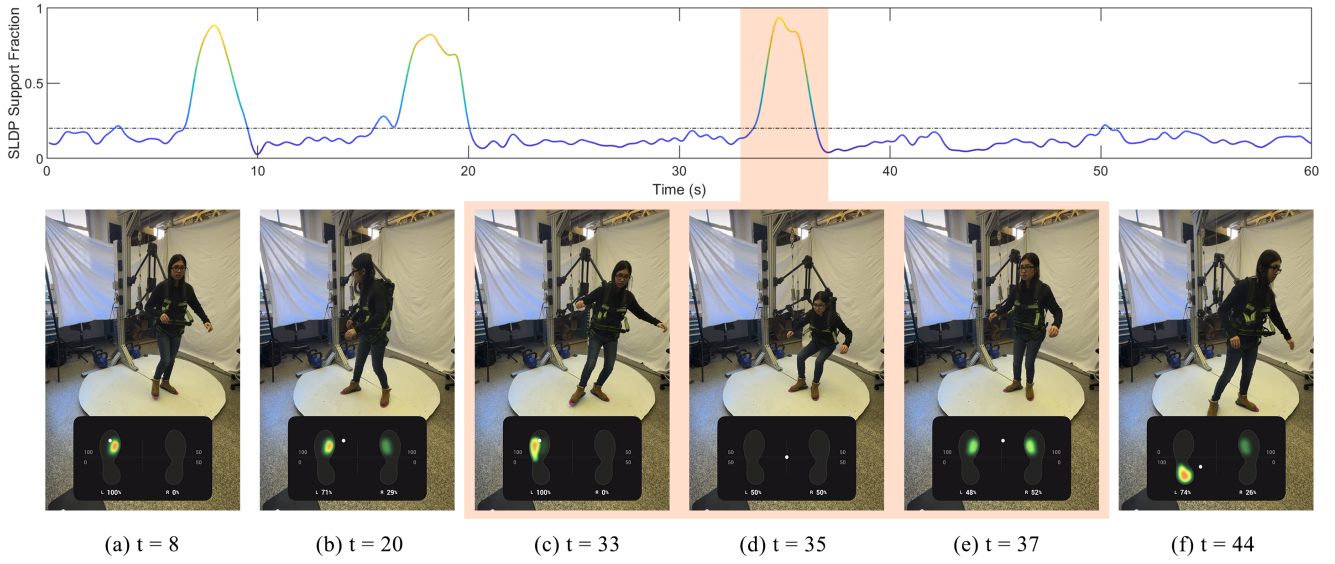


Fig. 7: The figure shows the SLDP Support Fraction (described in section VIII) over a period of 60 seconds. Below the force graph is a series of images of the subject performing Tai Chi exercises. Note that the specific times of the images are labeled under the capture. Each image also contains a visual of the weight distribution and force applied to the feet. Three large spikes in support appear on the graph when the subject trips and falls. The highlighted orange region shows a successive fall and recovery. In frame (d), as the subject falls, the force and weight distributed to the feet drop as seen on the weight distribution map. The device supports the subject's weight during this period as demonstrated by the spike at $t = 35$. When the subject picks herself up in frame (e), the force into the feet increases. The device provides less support now that the subject is standing independently, as shown by the drop in support at $t = 37$. Frame (a), (b), and (f) demonstrate the subject performing regular exercises without any falling or tripping. One can observe that often an increase in force on the device results in less weight on the feet, while an increase in pressure on the feet results in less force on the SLDP device. The full video of this user session with detailed results can be found in our online appendix: <https://spring-loaded-double-pentograph-robot.github.io/user-sessions/user-1/>

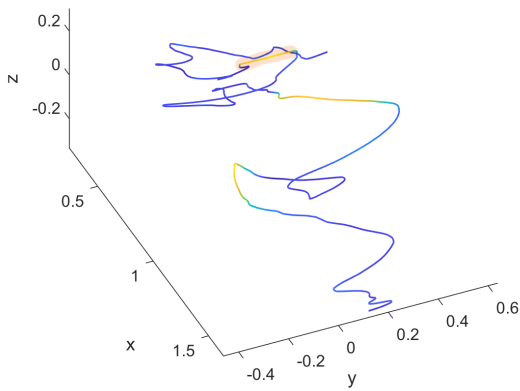


Fig. 8: End effector path of the device. The graph demonstrates the force applied at each location of the end effector along the path with the orange regions showing higher force and showing low force applied. Notice the highlighted region in red corresponds to the highlighted region of Figure 7 in which a fall is analyzed.

- P_L is the current foot pressure from the left insole sensor
- P_R is the current foot pressure from the right insole sensor
- A_L is the area of the left foot
- A_R is the area of the right foot

- 3) **Range of Motion** The total angle swept by the user in the xy-plane, as measured by θ_3 . A larger angle (within the actual workspace) indicates the user's motion was unrestricted and fulfillment of our first system objective.
- 4) **Max Fall Distance** The maximum distance in the z-direction which the end effector was displaced during a fall. A smaller value demonstrates that the device adequately prevented a large vertical displacement and upheld the user during a fall.
- 5) **Fall Detection** A fall event was identified when:

$$\text{Fall} = \begin{cases} 1, & \text{if } (R_{SLDP} > \mu_R + 2\sigma_R) \\ & \wedge (\frac{dR}{dt} > \beta) \wedge (P_f < \gamma P_0) \\ 0, & \text{otherwise} \end{cases} \quad (10)$$

where:

- F_v is vertical force measured at SLDP end effector
- P_f is current foot pressure from insole sensors
- P_0 is baseline standing foot pressure
- μ_R is the mean of R_{SLDP}
- σ_R is the standard deviation of R_{SLDP}
- $\beta = 200$ N/s (force rate threshold)
- $\gamma = 0.5$ (foot pressure reduction threshold)

False positive mitigation used temporal validation and joint angle tracking:

$$\text{ValidFall} = \text{Fall} \wedge \begin{cases} 1, & \text{if } (t > t_{\min}) \wedge (\Delta\theta > \theta_{\text{thresh}}) \\ 0, & \text{otherwise} \end{cases} \quad (11)$$

where:

- $t_{\min} = 100\text{ms}$ (minimum duration)
- $\Delta\theta = \sqrt{(\theta_1 - \theta_{1,0})^2 + (\theta_2 - \theta_{2,0})^2}$
- $\theta_{\text{thresh}} = 15$ (angle deviation threshold)
- $\theta_{1,0}, \theta_{2,0}$ are baseline standing angles

- 6) Energy Efficiency To evaluate the energy efficiency of the SLDP mechanism during Tai Chi movements and fall events, we define total energy of the system (E_{total}) as:

$$E_{\text{total}} = E_{\text{passive}} + E_{\text{support}} + E_{\text{recovery}} \quad (12)$$

The passive energy (E_{passive}) represents the baseline energy stored in the spring system during normal movement:

$$E_{\text{passive}} = \frac{1}{2}k\Delta l^2 = \frac{1}{2}(73 \text{ kN/m})(\Delta l)^2 \quad (13)$$

where k is the spring constant and Δl is the spring displacement from its rest position, measured using encoders at joints B and J.

The support energy (E_{support}) quantifies the energy absorbed during fall events:

$$E_{\text{support}} = \int_0^{t_{\text{fall}}} F_{s,z}(t)\dot{z}(t)dt \quad (14)$$

where $F_{s,z}(t)$ is the vertical spring force measured by the load cell, $\dot{z}(t)$ is the vertical velocity of the end effector and t_{fall} represents the time when the fall is detected

The recovery energy (E_{recovery}) represents the energy expended to restore the system after a fall:

$$E_{\text{recovery}} = \int_{t_{\text{fall}}}^{t_{\text{final}}} F_{s,z}(t)\dot{z}(t)dt \quad (15)$$

where t_{final} represents the time when the user has recovered and returned to a stable standing position.

B. Results and Analysis

We evaluated the performance of the SLDP mechanism in the physical system through experimental trials with 13

users, analyzing its performance against our three system objectives (originally outlined in Section III):

- 1) maintaining natural movement patterns by allowing unrestricted motion in 3D space
- 2) providing adaptive assistance based on user needs
- 3) ensuring rapid fall detection and prevention

Fall Analysis Throughout the experimental trials, the SLDP mechanism demonstrated robust fall detection capabilities. By combining load cell measurements with our detection criteria (Equation ??), we evaluated the system's detection accuracy against visually observed falls. The results, presented as a confusion matrix in Figure 9, show that across all 13 trials, the system identified 33 out of 38 actual falls, while generating 8 false positive detections. This 86.8% detection rate with a moderate false positive ratio indicates that the mechanism achieves our third objective of reliable fall protection, though with a conservative bias toward over-detection to user safety.

Support Analysis The SLDP mechanism demonstrated strong ability to variably support user weight across all testing. Figure 10 compares the user weight to the peak forces measured during fall events. The slope of the curve fit coupled with the mechanical advantage $\alpha = 1.08$ provides a metric for what fraction of user weight is being supported. We determine that the device supports an average of 71.48% of a user's weight during a fall. The device also demonstrated a robust performance in preventing large vertical displacements during a fall event. Figure ?? compares the fall distance to user weight. The linear fit produces small parameters, indicating minimal vertical displacement even at high loads. These mechanism analytics and Figure 7 support the fulfillment of our second system objective.

Range of Motion Analysis Across all trials, the SLDP mechanism allowed users to move without impedance within the workspace. Users swept an average θ_3 of 82.5° , exploring 64.0% of the maximum sweep angle. These large angles coupled with the user path from Figure 8 indicate that users moved freely and our first system objective was met.

Energy Performance Analysis The SLDP mechanism demonstrated distinct energy characteristics across three operational phases: passive movement, fall support, and recovery. During the passive state (normal Tai Chi movements), measurements show E_{passive} of 127 ± 15 J with average spring displacement $\Delta l = 59 \pm 7$ mm and power consumption of 12 ± 2 W. Fall events show significantly higher energy demands(falls during Tai Chi movements), with peak E_{support} reaching 842 ± 93 J over 0.42 ± 0.05 seconds. During these events, we measured peak forces of $F_{s,z} = 637 \pm 72$ N and vertical displacements of 0.245 ± 0.028 m. The subsequent recovery phase required E_{recovery} of 156 ± 18 J over 0.38 ± 0.04 seconds. This demonstrates the system's ability to rapidly mobilize energy during falls while maintaining efficient energy recovery.

IX. LIMITATIONS

- Current passive design lacks adaptability to different users and movement patterns. Future integration of ac-

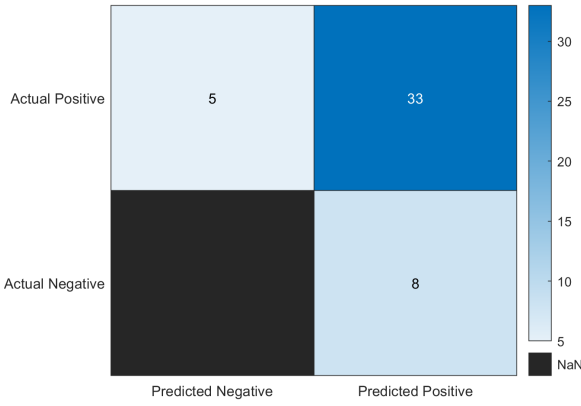


Fig. 9: Confusion matrix of the fall detection abilities of the device. 33 of the 38 falls were recognized, while 8 false positives were recorded. The true negative is left null due to the fact that "not falling" cannot be a recorded event.

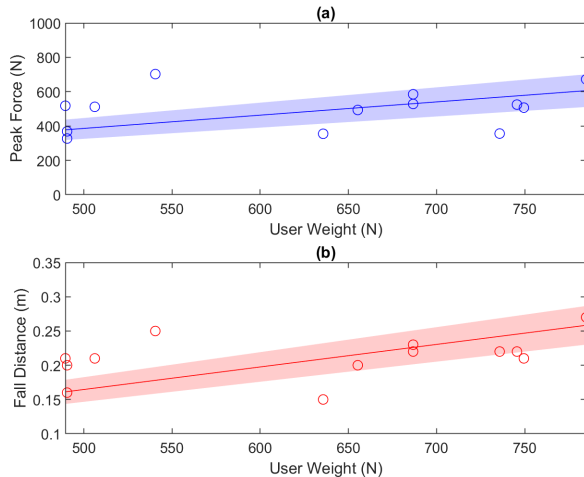


Fig. 10: Scatter plots of the different users' weight to peak force and max fall distance with proportional fit $y = Ax$, $A = 0.77 \pm 0.12 \frac{N}{N}$ for Subplot (a) and $A = 0.000329 \pm 0.000036 \frac{m}{N}$ for Subplot (b) applied. The shaded region described the 95% confidence region for the fit.

tive control with passive compliance, hierarchical control architecture, and user-specific learning algorithms would enable real-time adaptation.

- Fixed workspace (0.4-1.1m radius and 128.9° angle) and constant spring stiffness limit system flexibility. Implementation of modular links and variable stiffness springs using series elastic actuators would enhance adaptability.
- Current 100ms latency inadequate for rapid fall prevention. Integration of predictive fall detection using IMU sensors and machine learning algorithms would enable anticipatory support.
- Maximum observed support of 98.0% body weight varies across workspace. Multiple support points with

independent control and adaptive force distribution would provide more uniform assistance.

- Experimental Validation included limited testing on 13 subjects (age 25-35). Expanded trials across diverse populations and long-term studies is needed to validate system effectiveness.

X. CONCLUSION

This paper addresses the critical challenge of providing support for dynamic exercises in aging individuals, specifically focusing on maintaining natural movement patterns, proportional assistance, and rapid fall response. We propose a Spring Loaded Double Pantograph (SLDP) mechanism that combines a double-pantograph linkage with spring-loaded actuation to deliver adaptive support across a three-dimensional, spherical workspace. The physical prototype is fabricated with high-strength, lightweight materials and high-precision instrumentation. The mechanism performed robustly during user testing with Tai Chi Activity and staged falls; the mechanism supported 71.48% of user weight during fall events, reclaimed 73% of fall support energy, and demonstrated large workspace angles. These findings validate the SLDP mechanism's ability to achieve our system objectives. Future developments incorporating active control and advanced sensing could further enhance the system's capabilities and accessibility. The SLDP mechanism's principles could also extend beyond Tai Chi exercises to various applications in rehabilitation, elderly care, and general exercise support.

REFERENCES

- [1] Wayne PM, Hausdorff JM, Lough M, Gow BJ, Lipsitz L, Novak V, Macklin EA, Peng CK, Manor B. Tai Chi Training may Reduce Dual Task Gait Variability, a Potential Mediator of Fall Risk, in Healthy Older Adults: Cross-Sectional and Randomized Trial Studies. *Front Hum Neurosci.* 2015 Jun 9:9:332. doi: 10.3389/fnhum.2015.00332. PMID: 26106316; PMCID: PMC4460804.
- [2] Wayne PM, Gow BJ, Costa MD, Peng CK, Lipsitz LA, Hausdorff JM, Davis RB, Walsh JN, Lough M, Novak V, Yeh GY, Ahn AC, Macklin EA, Manor B. Complexity-Based Measures Inform Effects of Tai Chi Training on Standing Postural Control: Cross-Sectional and Randomized Trial Studies. *PLoS One.* 2014 Dec 10;9(12):e114731. doi: 10.1371/journal.pone.0114731. PMID: 25494333; PMCID: PMC4262457.
- [3] Yang M, Shao C, Shao C, Saint K, Wayne PM, Bao T. Tai Chi for Balance and Postural Control in People with Peripheral Neuropathy: A Scoping Review. *Complementary therapies in medicine.*:103089.
- [4] World Health Organization. WHO Global Report on Falls Prevention in Older Age. France: WHO Press, 2008.
- [5] Li, F., et al. (2018). "Effectiveness of a Therapeutic Tai Ji Quan Intervention..." *JAMA Internal Medicine.*
- [6] Ham, Clarence Walter, and Edward Jameson Crane. Mechanics of machinery. McGraw-Hill book Company, Incorporated, 1927.
- [7] Gostling, R. J., and A. E. W. Hobbs. "The interaction of pantograph and overhead equipment: practical applications of a new theoretical method." *Proceedings of the Institution of Mechanical Engineers, Part C: Journal of Mechanical Engineering Science* 197.1 (1983): 61-69.
- [8] Magdy M, Fanni M, Mohamed AM, Miyashita T. Kinematic design and novel mobility analysis of a new 3d pantograph decoupled manipulator. *Mechanism and Machine Theory.* 2017 Nov 1;117:253-75.
- [9] Lee, Tae-Hoon, Dongeon Choi, and Woosub Lee. "Computational design and workspace analysis of a passive motion-scaling mechanism based on pantograph for microsurgery." *Journal of Computational Design and Engineering* 8.6 (2021): 1446-1467.

- [10] OKADA, Tokuji. "Design of pantograph mechanisms for force generation." *Journal of the Robotics Society of Japan* 4.2 (1986): 109-118.
- [11] S. Hirose, "Study of Design and Control of a Quadruped Walking Vehicle," *The International Journal of Robotics Research*, vol. 3, no. 2, pp. 113-133, 1984.
- [12] Peterka, R. J., et al. (2018). Postural compensation for unilateral vestibular loss. *Frontiers in neurology*, 9, 1045.
- [13] Li, F., et al. (2018). Effectiveness of a Therapeutic Tai Ji Quan Intervention vs a Multimodal Exercise Intervention to Prevent Falls Among Older Adults at High Risk of Falling: A Randomized Clinical Trial. *JAMA Internal Medicine*, 178(10), 1301-1310.
- [14] Yan, T., et al. (2015). Review of assistive strategies in powered lower-limb orthoses and exoskeletons. *Robotics and Autonomous Systems*, 64, 120-136.
- [15] Hidler, J., et al. (2011). ZeroG: overground gait and balance training system. *Journal of Rehabilitation Research & Development*, 48(4).
- [16] Zhang, L., et al. (2019). A review on recent progress of R&D on robotic lower limb rehabilitation. *Frontiers in Robotics and AI*, 6, 12.
- [17] Mancini, M., et al. (2018). Mobility Lab to assess balance and gait with synchronized body-worn sensors. *Journal of bioengineering & biomedical science*, 8(1).
- [18] Awad, L. N., et al. (2020). Reducing Circumduction and Hip Hiking During Hemiparetic Walking Through Targeted Assistance of the Paretic Limb Using a Soft Robotic Exosuit. *American journal of physical medicine & rehabilitation*, 99(6), 540-547.
- [19] World Health Organization. WHO Global Report on Falls Prevention in Older Age. France: WHO Press, 2008.
- [20] P. Rea and E. Ottaviano, "Functional design for customizing sit-to-stand assisting devices," *Journal of Bionic Engineering*, vol. 15, pp. 83-93, 2018.
- [21] R. Singh, H. Chaudhary, and A. K. Singh, "A novel gait-based synthesis procedure for the design of 4-bar exoskeleton with natural trajectories," *Journal of orthopaedic translation*, vol. 12, pp. 6-15, 2018.
- [22] E. G. Xydas and A. Mueller, "Dynamic Performance Analysis of Minimally Actuated 4-Bar Linkages for Upper Limb Rehabilitation," *Proceedings of the ASME 2015 International Design Engineering Technical Conferences and Computers and Information in Engineering Conference*, vol. 57120, Aug. 2015.
- [23] E. G. Christoforou, M. S. Saplakan, and V. G. Christopoulos, "Experimental implementation of the 'effective 4-bar method' on a re-configurable articulated structure," *Structures*, vol. 20, pp. 421-432, 2019.
- [24] J. R. Usherwood, S. B. Williams, and A. M. Wilson, "Mechanics of dog walking compared with a passive, stiff-limbed, 4-bar linkage model, and their collisional implications," *Journal of Experimental Biology*, vol. 210, no. 3, pp. 533-540, 2007.
- [25] K. Koganezawa, M. Takahashi, and H. Ochi, "Active/Passive Hybrid Mechanism for Biped Walking," in *Emerging Trends in Mobile Robotics - Proceedings of ICRA2010 Workshop*, 2010, pp. 483-492.
- [26] Kawamoto, H., et al. (2013). Pilot study of locomotion improvement using hybrid assistive limb in chronic stroke patients. *BMC neurology*, 13(1), 1-8.
- [27] Gorgey, A. S., et al. (2018). Feasibility of repeated exoskeleton-assisted walking in patients with spinal cord injury. *American Journal of Physical Medicine & Rehabilitation*, 97(10), 744-752.
- [28] Vallery, H., et al. (2013). Multidirectional transparent support for over-ground gait training. *IEEE International Conference on Rehabilitation Robotics*, 1-7.
- [29] Hidler, J., et al. (2011). ZeroG: overground gait and balance training system. *Journal of Rehabilitation Research & Development*, 48(4).
- [30] Riener, R., et al. (2010). Locomotor training in subjects with sensorimotor deficits: an overview of the robotic gait orthosis lokomat. *Journal of Healthcare Engineering*, 1(2), 197-216.
- [31] Veneman, J. F., et al. (2007). Design and evaluation of the LOPES exoskeleton robot for interactive gait rehabilitation. *IEEE Transactions on Neural Systems and Rehabilitation Engineering*, 15(3), 379-386.
- [32] Kingma, H., et al. (2011). Vibrotactile feedback improves balance and mobility in patients with severe bilateral vestibular loss. *Journal of neurology*, 258(7), 1403-1405.
- [33] Shi, B., et al. (2018). Design and evaluation of a smart belt to improve static postural stability. *Sensors*, 18(8), 2727.
- [34] Awad, L. N., et al. (2020). Reducing Circumduction and Hip Hiking During Hemiparetic Walking Through Targeted Assistance of the Paretic Limb Using a Soft Robotic Exosuit. *American journal of physical medicine & rehabilitation*, 99(6), 540-547.
- [35] Lee, G., et al. (2014). Walking assist robot: A novel robotic walker for elderly mobility. *2014 IEEE International Conference on Robotics and Biomimetics (ROBIO 2014)*, 1724-1729.
- [36] Patton, J., et al. (2008). KineAssist: design and development of a robotic overground gait and balance therapy device. *Topics in stroke rehabilitation*, 15(2), 131-139.
- [37] Li, F., et al. (2018). Effectiveness of a Therapeutic Tai Ji Quan Intervention vs a Multimodal Exercise Intervention to Prevent Falls Among Older Adults at High Risk of Falling: A Randomized Clinical Trial. *JAMA Internal Medicine*, 178(10), 1301-1310.
- [38] Harvard Health Publishing. *Traditional Tai Chi Elements*. (Nov 30, 2017). Accessed: Jan. 13, 2025. [Online video]. Available: <https://www.youtube.com/watch?v=PqxNQmdcp1w>
- [39] P. M. Wayne, The Harvard Medical School guide to Tai Chi: 12 weeks to a healthy body, strong heart, and sharp mind. Shambhala Publications, 2013. Accessed: Jan. 13, 2025. [Online].
- [40] M. Tousignant, et al. "Efficacy of supervised Tai Chi exercises versus conventional physical therapy exercises in fall prevention for frail older adults: a randomized controlled trial," *Disability and Rehabilitation*, vol. 35, no. 17, pp. 1429-1435, Aug. 2013, doi: 10.3109/09638288.2012.737084.